Cluster states and monopole transitions in ^{16}O

Yoshiko Kanada-En'yo
Department of Physics, Kyoto University, Kyoto 606-8502, Japan
(Received 1 August 2013; revised manuscript received 12 December 2013; published 4 February 2014)

Cluster structures and monopole transitions in positive parity states of ^{16}O are investigated based on the generator coordinate method calculation of an extended ^{12}C+α cluster model. The ground and excited states of a ^{12}C cluster are taken into account by using ^{12}C wave functions obtained with the method of antisymmetrized molecular dynamics. The 0_2^+ state of ^{16}O and its rotational members, the 2_1^+ and 4_1^+ states, are described well by the cluster states dominated by the ^{12}C(0_1^+)+α structure. Above the ^{12}C(0_2^+)+α threshold energy, I obtain a 0^+ state having the ^{12}C(0_2^+)+α cluster structure, which is considered to be a candidate for the 4α cluster gas state. The band structures are discussed based on the calculated $E2$ transition strength. Isoscalar monopole excitations from the ground state are also discussed.

DOI: 10.1103/PhysRevC.89.024302 PACS number(s): 21.10.−k, 21.60.Gx, 23.20.−g

I. INTRODUCTION

Cluster structure is one of the essential features of nuclei as well as a mean-field feature. Well-developed cluster structures have been known, in particular, in excited states of stable light nuclei and also discovered in unstable nuclei. In recent years, a new type of cluster state, an α cluster gas state, has been suggested in light $Z = N$ nuclei [1–7]. It has been proposed that 2α and 3α cluster gas states are realized in the 0_1^+ state of ^{8}Be and the 0_2^+ state of ^{12}C, where all α clusters are almost freely moving in a dilute density like a gas. It is a challenging problem to search for such cluster gas states in other nuclei. For instance, the possibility of α cluster gas states in $Z = N = 2n$ nuclei up to ^{40}Ca was discussed in a systematic study with a nonmicroscopic cluster model, which suggested that α cluster gases may appear in the energy region near the corresponding n-α breakup threshold consistently with the Ikeda threshold rule [3]. Cluster gas states including non-α clusters or those around a core nucleus were also suggested in excited states of ^{11}B, ^{8}He, and ^{10}Be [8–15].

Recently, the search for the 4α cluster gas state in excited states of ^{16}O has been performed in experimental and theoretical works [5,6,16]. The semimicroscopic 4α calculation by Funaki *et al.* suggested that the ^{16}O(0_6^+) state near the 4α threshold has the large ^{12}C(0_2^+) + α component and is a candidate for the dilute 4α cluster gas state [5,6]. It is also an interesting problem to assign band members of the cluster gas state to clarify the property of the cluster gas, especially, stability against rotation as discussed in Refs. [17,18].

^{16}O is a double closed-shell nuclei and its ground state is dominated by p-shell closed configuration, while there exist many excited states that are difficult to be described by a simple shell model. Semimicroscopic and microscopic ^{12}C+α cluster models [19–21] were applied to study excited states of ^{16}O and it has been shown that many excited states can be described by ^{12}C+α cluster structures. For instance, in the calculation with the ^{12}C+α orthogonality condition model (OCM) [19], a semimicroscopic cluster model [22], the 0_2^+ state of ^{16}O and its rotational band members, the 2_1^+ and 4_1^+ states, are described by the cluster state having the dominant ^{12}C(0_1^+)+α component. Moreover, the ^{16}O(0_3^+) state is considered to mainly have the ^{12}C(2_1^+)+α component. These results are supported also by 4α-OCM calculations [5,6,23]. Thus, many excited states up to ∼14 MeV are considered to be weak-coupling ^{12}C+α cluster states having large components of ^{12}C(0_1^+)+α, ^{12}C(2_1^+)+α, and so on. The cluster structures of these excited states are supported by the experimental data of $E2$ and monopole transition strengths as well as the α-decay widths [19,20,24].

Above these ^{12}C+α cluster states, a 4α cluster state was predicted at the energy near the 4α and ^{12}C(0_2^+)+α threshold energies by Funaki *et al.* with the 4α-OCM [5,6]. This state has the large ^{12}C(0_2^+)+α component, that is, the 3α cluster gas state of the ^{12}C(0_2^+) with an additional α around the 3α gas. The large occupation probability of 4 α particles in the same 0S and low-momentum orbit was demonstrated by the analysis of the 4α-OCM wave function.

In spite of the success of those calculations with the semimicroscopic cluster models such as the ^{12}C+α-OCM and the 4α-OCM, there is no microscopic calculation that can reproduce the excitation energies of the cluster states in ^{16}O. The microscopic calculations with the resonating group method (RGM) [25] and the generator coordinate method (GCM) [26] of ^{12}C+α cluster models [20,21] failed to reproduce the experimental excitation energy of the 0_2^+ at 6.05 MeV. They largely overestimated it by a factor 2–3 as $E_x(0_2^+) \sim 16$ MeV. One of the most crucial problems in microscopic calculations using effective nuclear forces for ^{16}O is the underbinding problem of ^{12}C relative to ^{16}O, or in other words, the overbinding problem of ^{16}O relative to ^{12}C.

My aim is to investigate cluster structures of excited states of ^{16}O. In particular, I search for a highly excited 0^+ state having the ^{12}C(0_2^+)+α structure, which may be the candidate for the 4α gas state. I perform the GCM calculation of an extended ^{12}C+α model. In the present calculation, I adopt the ^{12}C wave functions obtained with the variation after the parity and angular-momentum projections (VAP) in the framework of antisymmetrized molecular dynamics (AMD) [27,28]. As shown in the previous works on ^{12}C [29,30], the AMD+VAP calculation succeeded in describing well the structures of ground and excited states of ^{12}C, such as the developed 3α-cluster structure in the excited states as well as the ground state properties. The binding energy of ^{12}C was improved because of the energy gain of the spin-orbit

force due to the mixing of $p_{3/2}$-shell configurations. I use the same effective nuclear force used in the previous study of ^{12}C, that it, the MV1 force [31] containing the phenomenological three-body repulsive force to avoid the overshooting problem of the binding energy in heavier nuclei. To take into account the ground and excited states of ^{12}C I superpose the ^{12}C AMD wave functions and approximately perform the double projection, that is, the angular-momentum projection of the subsystem ^{12}C and that of the total system. Isoscalar monopole excitations in ^{16}O are also discussed.

This paper is organized as follows. In the next section, I explain the formulation of the present calculation. The results are shown in Sec. III, and isoscalar monopole excitations are discussed in Sec. IV. Finally, a summary and outlook are given in Sec. V.

II. FORMULATION

A. ^{12}C(AMD)+αGCM calculation for ^{16}O

The ground and excited states of ^{16}O are described by using an extended ^{12}C+α cluster wave function. To describe intercluster motion, the distance d between the mean positions of ^{12}C and α centers is treated as the generator coordinate, and the ^{12}C+α wave functions with different d values are superposed. The α cluster is written by the $(0s)^4$ harmonic oscillator wave function $\Phi_\alpha(3\mathbf{S}/4)$ which is localized around the position $3\mathbf{S}/4$ with $\mathbf{S}=(0,0,d)$. The ^{12}C cluster is localized around $-\mathbf{S}/4$ and described by the superposition of AMD wave functions.

An AMD wave function for the ^{12}C cluster localized around the origin is given as follows:

$$\Phi^{\rm AMD}_{^{12}{\rm C}}(\mathbf{Z}) = \frac{1}{\sqrt{A_C!}}\mathcal{A}_C\{\varphi_1,\varphi_2,...,\varphi_{A_C}\}, \quad (1)$$

$$\varphi_i = \phi_{\mathbf{X}_i}\chi_i\tau_i, \quad (2)$$

$$\phi_{\mathbf{X}_i}(\mathbf{r}_j) = \left(\frac{2\nu}{\pi}\right)^{4/3}\exp\left\{-\nu\left(\mathbf{r}_j-\frac{\mathbf{X}_i}{\sqrt{\nu}}\right)^2\right\}, \quad (3)$$

$$\chi_i = \left(\frac{1}{2}+\xi_i\right)\chi_\uparrow + \left(\frac{1}{2}-\xi_i\right)\chi_\downarrow. \quad (4)$$

Here A_C is the mass number of ^{12}C, $A_C=12$, and the operator $\mathcal{A}_C$ is the antisymmetrizer of the A_C nucleons. The wave function $\Phi^{\rm AMD}_{^{12}{\rm C}}(\mathbf{Z})$ is written by a Slater determinant of single-particle wave functions φ_i, each of which is given by a product of the spatial ($\phi_{\mathbf{X}_i}$), the intrinsic spin (χ_i), and isospin (τ_i) functions. The isospin function is fixed to be up (proton) or down (neutron). The spatial part $\phi_{\mathbf{X}_i}$ is written by the Gaussian wave packet localized around the position $\mathbf{X}_i$ in the phase space. Accordingly, an AMD wave function is expressed by a set of variational parameters, $\mathbf{Z}\equiv\{\mathbf{X}_1,\mathbf{X}_2,\ldots,\mathbf{X}_{A_C},\xi_1,\xi_2,\ldots,\xi_{A_C}\}$, which expresses an AMD configuration of the ^{12}C cluster. The mean position $\{\mathbf{X}_1+\mathbf{X}_2+\cdots+\mathbf{X}_{A_C}\}/A_C$ of ^{12}C mass center is set on the origin.

The ^{12}C wave function is shifted from the origin to the position $-\mathbf{S}/4$ by shifting the Gaussian center parameters $\mathbf{X}_i\to\mathbf{X}_i-\mathbf{S}/4$. The shifted ^{12}C AMD wave function is denoted by $\Phi^{\rm AMD}_{^{12}{\rm C}}(-\mathbf{S}/4;\mathbf{Z})$. A wave function $\Phi^{\rm AMD}_{^{12}{\rm C}}(-\mathbf{S}/4;\mathbf{Z})$ corresponds to the ^{12}C cluster around $-\mathbf{S}/4$ having an intrinsic wave function specified by the set of parameters $\mathbf{Z}$. To construct the angular-momentum eigenstate of the subsystem ^{12}C projected from the intrinsic state, it is necessary to superpose rotated states of the intrinsic wave function. For a configuration $\mathbf{Z}=\mathbf{Z}^{(k)}$ (k is the label for the configuration) of the ^{12}C AMD wave function, I prepare rotated states $R^{\rm sub}(\Omega')\Phi^{\rm AMD}_{^{12}{\rm C}}(-\mathbf{S}/4;\mathbf{Z}^{(k)})$ of the subsystem ^{12}C. Here $R^{\rm sub}(\Omega')$ is the operator of the Euler angle Ω' rotation of the subsystem around $-\mathbf{S}/4$. A wave function of ^{16}O is given by performing the antisymmetrization of all nucleons and the parity and angular-momentum projections,

$$\Phi^{J\pi K}_{^{12}{\rm C}+\alpha}(d,\Omega'_j,\mathbf{Z}^{(k)}) = P^{J\pi}_{MK}\mathcal{A}\left\{R^{\rm sub}(\Omega')\Phi^{\rm AMD}_{^{12}{\rm C}}(-\mathbf{S}/4;\mathbf{Z}^{(k)})\cdot\Phi_\alpha(3\mathbf{S}/4)\right\}. \quad (5)$$

Here $\mathcal{A}$ is the antisymmetrizer for all sixteen nucleons and $P^{J\pi}_{MK}$ is the parity(π) and angular-momentum projection operator for the total system.

I superpose ^{16}O wave functions constructed from the ^{12}C AMD wave function and the α cluster wave function. Each ^{16}O wave function is specified by the AMD configuration $\mathbf{Z}^{(k)}$, the rotation angle Ω'_j for the ^{12}C cluster, and the intercluster distance d_i. Then the final ^{16}O wave function in the present ^{12}C(AMD)+αGCM model is written as follows:

$$\Psi^{J^\pi_n}_{\rm AMD+\alpha GCM} = \sum_{K,i,j,k} c^{J^\pi_n}(K,i,j,k)\Phi^{J\pi K}_{^{12}{\rm C}+\alpha}(d_i,\Omega'_j,\mathbf{Z}^{(k)}). \quad (6)$$

The coefficients $c^{J^\pi_n}(K,i,j,k)$ for the J^π_n state are treated as independent parameters and they are determined by solving the Hill-Wheeler equation as done in the GCM [26]. In principle, the superposition of rotated states of the ^{12}C cluster is equivalent to the so-called "double projection," in which the angular-momentum projections are done for the subsystem ^{12}C and also for the total system. It corresponds to taking into account different spin states of the ^{12}C cluster. In the practical calculation, however, I use only a limited number of the rotation angle Ω'_j and it is an approximated method of the double projection. By superposing several AMD configurations of ^{12}C, excited states as well as the ground state of the ^{12}C cluster are incorporated. The details of the AMD configurations of ^{12}C are explained later.

For general nuclei, I can consider the extended cluster model "AMD+αGCM," in which a core nucleus is written by AMD wave functions and relative motion between an α cluster and the core is taken into account by superposing core-α cluster wave functions with various values of the distance d. Based on a similar concept, core+n cluster models have been already used to describe a valence neutron motion around the core expressed by AMD wave functions in the studies of neutron-rich nuclei. First a ^{10}Be(AMD)+nGCM model without the angular-momentum projection of the subsystem has been adopted to ^{11}Be [27], and recently, ^{30}Ne(AMD)+nGCM and ^{12}Be(AMD)+nGCM models have been applied to ^{31}Ne and ^{13}Be [32,33].

B. Wave functions of ^{12}C

In the previous work on ^{12}C [29,30], the AMD+VAP method has been applied to ^{12}C and it has been proven to describe well the structures of the ground and excited states in ^{12}C. To describe the ^{12}C cluster in the present ^{12}C(AMD)+αGCM calculation, I use the intrinsic wave functions of ^{12}C obtained with the AMD+VAP in Ref. [30].

I here briefly explain the AMD+VAP method [29,30]. More details of the method are described in Ref. [30]. As mentioned before, the AMD wave function of ^{12}C explained in Eq. (1) is specified by the set of parameters, $\mathbf{Z} = \{\mathbf{X}_1,\mathbf{X}_2,\ldots,\mathbf{X}_{A_C},\xi_1,\xi_2,\ldots,\xi_{A_C}\}$. In the AMD framework, these are treated as variational parameters and determined by the energy variation. In the AMD+VAP method, the energy variation is performed after the spin-parity projection. Namely, the parameters $\mathbf{X}_i$ and $\xi_i (i = 1 \sim A)$ are varied to minimize the energy expectation value of the Hamiltonian, $\langle\Phi|H|\Phi\rangle/\langle\Phi|\Phi\rangle$, with respect to the spin-parity eigenwave function $\Phi = P^{J\pi}_{MK}\Phi^{\rm AMD}_{^{12}{\rm C}}(\mathbf{Z})$ projected from the AMD wave function of ^{12}C. Then the optimum AMD wave function $\Phi^{\rm AMD}_{^{12}{\rm C}}(\mathbf{Z}^{J^\pi_1})$, which approximately describes the intrinsic wave function for the J^π_1 state, is obtained. For higher J^π_n states, the variation is done for the component orthogonal to the lower J^π states. For each $J(k)^{\pi(k)}_{n(k)}$, the optimum parameters $\mathbf{Z}^{(k)}$ are obtained. Here (k) is the label for the AMD configuration for the $J(k)^{\pi(k)}_{n(k)}$ state. After the VAP procedure, final wave functions for J^π states are expressed by the superposition of the spin-parity eigenwave functions projected from all the intrinsic wave functions $\Phi^{\rm AMD}_{^{12}{\rm C}}(\mathbf{Z}^{(k)})$ as

$$\Psi^{J_n,\pi}_{^{12}{\rm C}} = \sum_{K,k} c^{J^\pi_n}_{^{12}{\rm C}}(K,k)\left|P'^{J\pi}_{MK}\Phi^{\rm AMD}_{^{12}{\rm C}}(\mathbf{Z}^{(k)})\right\rangle, \tag{7}$$

where the coefficients $c^{J^\pi_n}_{^{12}{\rm C}}(K,k)$ are determined by solving the Hill-Wheeler equation, i.e., the diagonalization of the norm and Hamiltonian matrices.

In the previous study of ^{12}C, totally, 23 AMD configurations $\Phi^{\rm AMD}_{^{12}{\rm C}}(\mathbf{Z}^{(k)})$ $(k = 1,\ldots,23)$ are obtained by the energy variation for $J(k)^{\pi(k)}_{n(k)} = 0^+_1,0^+_2,0^+_3,1^+_1,2^+_1,2^+_2,2^+_3,\ldots,1^-_1,2^-_1,3^-_1,\ldots,$ and they are adopted as basis wave functions of the final wave functions of ^{12}C. In the present ^{12}C(AMD)+αGCM calculation, I adopt only three basis wave functions to save the computational cost. In order to take into account the ground and second 0^+ states of ^{12}C, I choose two basis wave functions of $J(k)^{\pi(k)}_{n(k)} = 0^+_1,0^+_2$ for $k = 1,2$. I also adopt the basis wave function of $J(k)^{\pi(k)}_{n(k)} = 1^-_1$ for the third basis wave function $(k = 3)$ to reasonably reproduce the energy levels of positive- and negative-parity states of ^{12}C. The intrinsic density of these three basis wave functions are shown in Fig. 1. The ground state has the compact structure of 3α with a mixing of the $p_{3/2}$-shell closure component, while the 0^+_2 and 1^-_1 states show developed 3α cluster structures.

The energy levels of ^{12}C obtained with the truncated model space of three bases are shown in Fig. 2 compared with those with full 23 basis wave functions and experimental ones. With the truncation, I get reasonable reproduction of the energy levels of many positive and negative parity states though the full 23 basis wave functions give better results, in particular, for excited states. The reason for $\sim$2 MeV higher energies of the 0^+_2 and 1^-_1 states with the three bases than those with the full bases is that these states gain their energy by the superposition of various configurations of the 3α cluster.

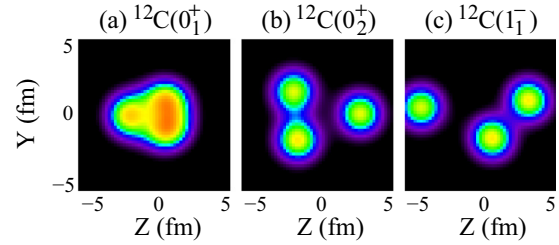

FIG. 1. (Color online) Density distribution of the intrinsic states of (a) ^{12}C(0^+_1), (b) ^{12}C(0^+_2), and (c) ^{12}C(1^-_1) calculated with the AMD+VAP [30]. The orientation of an intrinsic state is chosen so as to satisfy $\langle x^2\rangle \leqslant \langle y^2\rangle \leqslant \langle z^2\rangle$ and $\langle xy\rangle = \langle yz\rangle = \langle zx\rangle = 0$. The horizontal and vertical axes are set to the z and y axes, respectively. Densities are integrated with respect to the x axis.

I also calculate the overlap $\mathcal{N}(^{16}{\rm O}(J^\pi_n);^{12}{\rm C}(0^+_n)+\alpha;d)$ of the ^{16}O wave function obtained by the ^{12}C(AMD)+αGCM and the ^{12}C(0^+_n)+α wave function having a certain distance d,

$$\Phi^{J\pi}_{^{12}{\rm C}(0^+_n)+\alpha}(d) \equiv n_0 P^{J\pi}_{00}\mathcal{A}\left\{\sum_k c^{0^+_n}_{^{12}{\rm C}}(K=0,k)P'^{0}_{00}\Phi^{\rm AMD}_{^{12}{\rm C}}(-\mathbf{S}/4;\mathbf{Z}^{(k)}) \times \Phi_\alpha(3\mathbf{S}/4)\right\}, \tag{8}$$

$$\mathcal{N}\left(^{16}{\rm O}\left(J^\pi_n\right);^{12}{\rm C}(0^+_n)+\alpha;d\right) \equiv \left|\left\langle\Psi^{J^\pi_n}_{\rm AMD+\alpha GCM}\middle|\Phi^{J\pi}_{^{12}{\rm C}(0^+_n)+\alpha}(d)\right\rangle\right|^2. \tag{9}$$

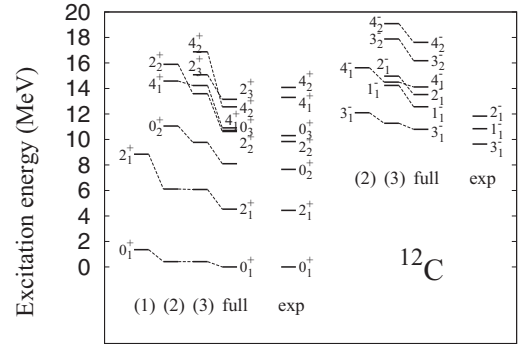

FIG. 2. Energy spectra of ^{12}C calculated with the AMD+VAP using three basis AMD wave functions $\Phi^{\rm AMD}_{^{12}{\rm C}}(\mathbf{Z}^{(k)})$ obtained by the energy variation for $J(k)^{\pi(k)}_{n(k)} = 0^+_1,0^+_2$ and 1^-_1 with $k = 1,2$, and 3, respectively, and that using the full 23 basis AMD wave functions. The 0^+_1 energy calculated with the 23 bases is adjusted to 0 and the relative energies are plotted. The energies calculated using (1) one basis $(k = 1)$, (2) two bases $(k = 1,2)$, (3) three bases $(k = 1,2,3)$, and (full) the full bases are shown. The excitation energies of the experimental data are also shown.

Here n_0 is the normalization factor to satisfy

$$\left|\left\langle \Phi^{J\pi}_{^{12}\mathrm{C}(0^+_n)+\alpha}(d)\middle|\Phi^{J\pi}_{^{12}\mathrm{C}(0^+_n)+\alpha}(d)\right\rangle\right|^2 = 1, \qquad (10)$$

and the Ω' integration in the operator P'^{0}_{00} of the $J=0$ angular-momentum projection of the subsystem is approximated by the sum of the finite number mesh points, $P'^{0}_{00} = \sum_j R^{\mathrm{sub}}(\Omega'_j)$. In the present work, I calculate the overlap only with the $^{12}\mathrm{C}(0^+_n)$-cluster wave function because of the approximation with the finite points of the Euler angle Ω'_j for the rotation of subsystem $^{12}\mathrm{C}$.

C. Parameters in numerical calculations

The width parameter ν of the $^{12}\mathrm{C}$ cluster is $\nu = 0.19$ fm^{-2} which was used in the previous work on $^{12}\mathrm{C}$ in Ref. [30]. The width parameter of the α cluster is taken to be the same value $\nu = 0.19$ fm^{-2} because the center of mass motion can be exactly extracted when a common width parameter is used for all clusters.

For the intercluster distance between $^{12}\mathrm{C}$ and α, six points $d_i = 1.2, 2.4, 3.6, \ldots, 7.2$ fm are chosen. The choice of $d_i \leqslant 7.2$ fm corresponds to a kind of bound state approximation. In the angular-momentum projection of the total system, the integration of the Euler angle $\Omega = (\theta_1, \theta_2, \theta_3)$ is numerically performed by the summation of mesh points (23,46,23) of the angles $(\theta_1, \theta_2, \theta_3)$.

For the intrinsic states of $^{12}\mathrm{C}$ labeled by (k), three AMD configurations are adopted. For each intrinsic state (k) at the distance d_i, seventeen rotated states $R^{\mathrm{sub}}(\Omega'_j)\Phi^{\mathrm{AMD}}_{^{12}\mathrm{C}}(-\mathbf{S}/4; \mathbf{Z}^{(k)})$ $(j = 1, \ldots, 17)$ are constructed. The Euler angle $\Omega' = (\theta'_1, \theta'_2, \theta'_3)$ is chosen to be $\theta'_1 = (0, \pi/4, \pi/2, 3\pi/4, \pi)$ and $\theta'_2 = (0, \pi/4, \pi/2, 3\pi/4, \pi)$. I omit the points $\theta'_2 = (5\pi/4, 3\pi/2, 7\pi/4)$ in the region $\pi < \theta'_2 < 2\pi$ to save the numerical cost. This is valid when the intrinsic state has the symmetry such as an isosceles triangle 3α configuration. θ'_3 is fixed to be $\theta'_3 = 0$ because the rotation θ'_3 is effectively done by the K projection in the angular-momentum projection of the total system because of the rotational invariance of the α cluster. As for the K mixing, I truncate the $|K| \geqslant 4$ components.

III. RESULTS

A. Effective nuclear interaction

In the present calculation of the $^{12}\mathrm{C}$(AMD)+αGCM, I use the same effective nuclear interaction with the same parameters as those used in the previous calculation of $^{12}\mathrm{C}$ [30]. It is the MV1 force [31] for the central force supplemented by the two-body spin-orbit force with the two-range Gaussian form the same as that in the G3RS force [34]. The Coulomb force is approximated using a seven-range Gaussian form. The Majorana, Bartlett, and Heisenberg parameters in the MV1 force are $m = 0.62$, $b = 0$, and $h = 0$, respectively, and the spin-orbit strengths are taken to be $u_I = -u_{II} = 3000$ MeV.

B. Energy levels of 0^+ states

In the preceding studies [5,6,19–21,23], developed cluster structures were suggested in excited 0^+ states of $^{16}\mathrm{O}$. It is considered that the ground state of 0^+_1 is dominated by the doubly closed-shell structure, while the 0^+_2 state has the $^{12}\mathrm{C}(0^+_1)+\alpha$ structure. The 0^+_3 state is suggested to have the $^{12}\mathrm{C}(2^+_1)+\alpha$ component. In the 4α-OCM calculation, it was suggested that the 0^+_4 mainly has the $^{12}\mathrm{C}(0^+_1)+\alpha$ structure with higher nodal behavior of α cluster around $^{12}\mathrm{C}$ and the 0^+_5 contains the $^{12}\mathrm{C}(1^-_1)+\alpha$ component. In the study with the 4α-OCM calculation by Funaki *et al.* [5,6], the 0^+_6 state having the $^{12}\mathrm{C}(0^+_2)+\alpha$ structure was suggested and regarded as the 4α cluster gas state. They proposed that the experimental 0^+_6 state at 15.1 MeV is a candidate for the 4α cluster gas state.

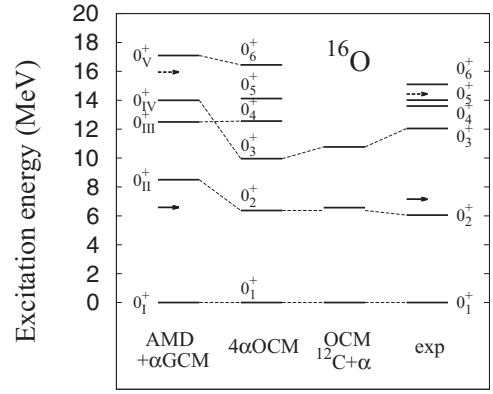

FIG. 3. Excitation energies of 0^+ states in $^{16}\mathrm{O}$ calculated with the present $^{12}\mathrm{C}$(AMD)+αGCM (AMD+αGCM) and those of the 4α-OCM and $^{12}\mathrm{C}+\alpha$-OCM from Refs. [5,19]. The experimental energy levels of 0^+ states are taken from Refs. [16,35]. The $^{12}\mathrm{C}(0^+_1)+\alpha$ and $^{12}\mathrm{C}(0^+_2)+\alpha$ threshold energies are plotted by solid and dashed arrows, respectively.

The energy levels of 0^+ states of $^{16}\mathrm{O}$ up to the fifth 0^+ state calculated with the $^{12}\mathrm{C}$(AMD)+αGCM calculation are shown in Fig. 3 compared with the experimental data. The theoretical energy levels with other theoretical calculations, 4α-OCM [5,6] and $^{12}\mathrm{C}+\alpha$-OCM [19], are also shown.

In the present result, the ground state (0^+_I) has mainly the doubly closed-shell structure with less development of cluster, while the second 0^+ state (0^+_{II}) is described mainly by the developed $^{12}\mathrm{C}(0^+_1)+\alpha$ structure. The cluster structure of the 0^+_{II} state is consistent with that of the preceding works and can be assigned to the experimental 0^+_2 state at 6.05 MeV. Above the second 0^+ state, I obtain the third 0^+ state (0^+_{III}) having further developed $^{12}\mathrm{C}(0^+_1)+\alpha$ structure and the fourth 0^+ state (0^+_{IV}) showing a feature of the $^{12}\mathrm{C}(2^+_1)+\alpha$ structure. The features of the 0^+_{III} and 0^+_{IV} states are consistent with the 0^+_4 and 0^+_3 states in the 4α-OCM calculation [5,6,24], respectively. The ordering of the 0^+_{III} and 0^+_{IV} is opposite to that of the 4α-OCM calculation. If I assign the 0^+_{IV} state to the 0^+_3 at 12.05 MeV, the experimental level spacing between the 0^+_2 and 0^+_3 state is reproduced well by the present calculation. For the 0^+_{III} state, the dominant $^{12}\mathrm{C}(0^+_1)+\alpha$ structure with an α far from the $^{12}\mathrm{C}(0^+_1)$ core is consistent with the 0^+_4 state in the 4α-OCM calculation which is assigned to the 0^+_4 state at 13.6 MeV from its relatively large width. The present calculation is a bound state approximation, and it is difficult to discuss the width in the present framework of AMD. Moreover, stability

of this state should be checked carefully by taking into account mixing of continuum states.

In the present calculation, I obtain the fifth 0^+ state (0^+_V) having the developed ^{12}C(0^+_2)+α structure. As discussed later, it has a large ^{12}C(0^+_2)+α component with an α cluster moving around the ^{12}C(0^+_2) cluster in the S-wave channel and it is consistent with the structure of the 4α cluster gas state in the 0^+_6 suggested by the 4α-OCM calculation. The 0^+_V state has a significant α-cluster amplitude about 4 $\sim$ 5 fm far from the ^{12}C(0^+_2) core. This is the same region of the α-cluster amplitude in the ^{12}C(0^+_2). Considering that the ^{12}C(0^+_2) has the 3α cluster gas feature and the fourth α is moving in the S wave in the same region of 3α clusters, the 0^+_V state can be regarded as a 4α cluster gas state similar to the 3α cluster gas in the ^{12}C(0^+_2).

The 0^+ energy spectra up to the 0^+_V in the present result correspond partially to the 0^+ states suggested by the 4α-OCM calculation. Considering the dominant component of each state, the present 0^+_{II} with the ^{12}C(0^+_1)+α component, the 0^+_{IV} with the ^{12}C(2^+_1)+α component, and the 0^+_V with the ^{12}C(0^+_2)+α component correspond to the 0^+_2, 0^+_3, and 0^+_6 states in the 4α-OCM. If I follow the assignments of Ref. [6] for these states to the experimental 0^+_2, 0^+_3, and 0^+_6 states, the level spacing between these three states (0^+_{II}, 0^+_{IV}, and 0^+_V) in the present result are in good agreement with the experimental one. The 0^+_{III} state having the higher nodal feature of ^{12}C(0^+_1)+α may correspond to the 0^+_4 in the 4α-OCM, but the energy position is relatively lower than the 0^+_{IV} with the ^{12}C(2^+_1)+α component, maybe, because of the overestimation of the ^{12}C(0^+_1)-^{12}C(2^+_1) level spacing in the present model space constructed by three basis AMD wave functions for the subsystem ^{12}C. The present result shows the state mixing in the 0^+_{III} and 0^+_{IV} states of the higher nodal ^{12}C(0^+_1)+α and the ^{12}C(2^+_1)+α components, indicating that these two components almost degenerate energetically. The details of the relative energy position of 0^+ states can be improved by taking into account full basis wave functions for ^{12}C. In the 4α-OCM, the 0^+_5 state with the ^{12}C(1^-_1)+α component is suggested, but there is no corresponding 0^+ state below the 0^+_V state in the present calculation. I only find the significant fraction of the ^{12}C(1^-_1)+α components in several 0^+ states around E_x $\sim$ 20 MeV, a few MeV higher than the 0^+_V state, but I cannot identify the ^{12}C(1^-_1)+α state as a single 0^+ state. The ordering of the 0^+_{II}, 0^+_{IV}, and 0^+_V states can be understood by the subsystem energy of the ^{12}C(0^+_1), ^{12}C(2^+_1), and ^{12}C(0^+_2). Similarly, the ^{12}C(1^-_1)+α state could be expected to exist in the energy region a few MeV higher than the ^{12}C(0^+_2)+α state from the energy difference of the subsystem states, ^{12}C(0^+_2) and ^{12}C(1^-_1). Our result is consistent with this naive expectation, but inconsistent with the 4α-OCM calculation [6,23,24] which suggests the ^{12}C(1^-_1)+α state at the much lower energy assigned to the experimental 0^+_5 from the α-decay width and the monopole strength. Probably, some effects could be missing in the present calculation.

The root-mean-square charge radii and monopole transition matrices $M(E0)$ for the 0^+ states are shown in Table I. The excited states tend to have large rms charge radii due to developed cluster structures compared with that of the ground state. In particular, the 0^+_{III} state with the higher nodal ^{12}C(0^+_1)+α structure and 0^+_V state with the ^{12}C(0^+_2)+α structure have about 1 fm larger radii than the ground state. The radius of the 0^+_V state is smaller than the 0^+_6 state of the 4α-OCM calculation. It may come from the smaller radius of ^{12}C(0^+_2) with the 3-basis AMD+VAP calculation than that with the 3α-OCM calculation [38]. Namely, the rms matter radius of ^{12}C(0^+_2) is 3.2 fm in the 3-basis AMD+VAP result (3.3 fm in the full 23-basis AMD+VAP) and 4.31 fm in the 3α-OCM calculation.

TABLE I. The charge radii (R_c), $E0$ transition matrix elements [$M(E0)$], and ratio ($P_{\text{E.W.}}$) to the EWSR of the isoscalar $E0$ transition that is 1/4 of the isoscalar monopole EWSR. The theoretical values are those calculated with the present ^{12}C(AMD)+αGCM, the 4α-OCM [24], and the ^{12}C+α-OCM [19]. The charge radius of a proton 0.887 fm [36] is used to evaluate the charge radii of 0^+ states in ^{16}O. Experimental data are taken from Refs. [35–37].

State	E_x (MeV)	R_c (fm)	$M(E0)$ (e fm^2)	$P_{\text{E.W.}}$ (%)
		^{12}C(AMD)+αGCM		
0^+_I	0.0	2.9		
0^+_{II}	8.5	3.5	4.0	5.4
0^+_{III}	12.5	3.9	3.5	6.4
0^+_{IV}	14.0	3.5	6.0	20
0^+_V	17.1	3.8	1.4	1.4
		Exp.		
0^+_1	0	2.70		
0^+_2	6.05		3.55(0.21)	3.5
0^+_3	12.05		4.03(0.09)	9.1
0^+_4	13.6			
0^+_5	14.01		3.3(0.7)	6.3
0^+_6	15.1			
		4α-OCM		
0^+_1	0	2.7		
0^+_2	6.37	3	3.9	4
0^+_3	9.96	3.1	3.9	6.3
0^+_4	12.56	4	2.4	3
0^+_5	14.12	3.1	2.6	3.9
0^+_6	16.45	5.6	1.0	0.7
		^{12}C+α-OCM		
0^+_1	0	2.5		
0^+_2	6.57	2.9	3.88	4.8
0^+_3	10.77	2.8	3.5	6.4

Those excited states with developed cluster structures also have significant monopole transition strength from the ground state. The transition strength to the 0^+_V state is relatively smaller than those to the lower 0^+ states. The present result is consistent with that of the 4α-OCM calculation in Ref. [24]. Detailed discussion of isoscalar monopole excitations is given in the next section.

C. $E2$ transition strength and band assignment

As mentioned above, the present result suggests the ^{12}C(0^+_2)+α structure in the 0^+_V state which is regarded as the candidate for the 4α cluster gas state. By analyzing the calculated $E2$ transition strength, I consider rotational band members from the ^{12}C(0^+_2)+α structure. The calculated

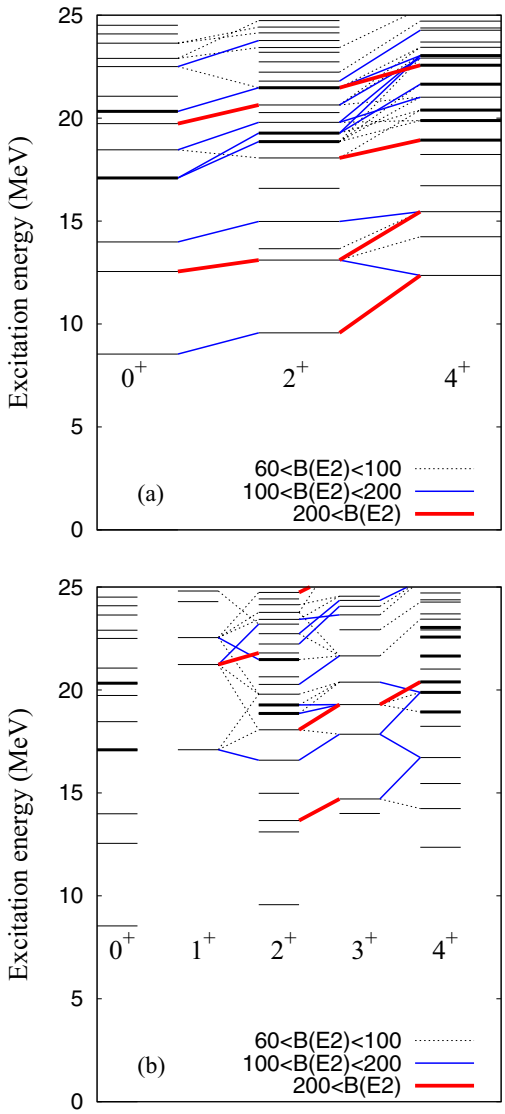

FIG. 4. (Color online) Calculated $E2$ transition strength in ^{16}O obtained with the ^{12}C(AMD)+αGCM. States having strong $E2$ transition with $60 < B(E2) < 100$ e^2 fm^4, $100 < B(E2) < 200$ e^2 fm^4, and $200 < B(E2)$ e^2 fm^4 are connected by dotted, thin (blue), and thick (red) lines, respectively. (a) $J^\pi = 0^+,2^+,4^+$ spectra and $4^+ \to 2^+$ and $2^+ \to 0^+$ transitions. (b) $J^\pi = 0^+,1^+,2^+,3^+,4^+$ spectra and $J^+ \to (J-1)^+$ transitions. The solid thick lines in the energy spectra are energy levels having significant ^{12}C(0_2^+)+α component.

$E2$ transition strength is shown in Fig. 4. The experimental and theoretical $B(E2)$ values for low-energy states are listed in Table II. For the lowest ^{12}C(0_1^+)+α cluster band consisting of the 0_2^+, 2_1^+, and 4_1^+ states, the present ^{12}C(AMD)+αGCM calculation reproduces reasonably the strong intraband $E2$ transitions within a factor 2. Twice larger $B(E2)$ values than the experimental data may suggest $\sim 20\%$ overestimation of the rms radii of these states which may come from the higher energy position relative to the ^{12}C(0_1^+)+α threshold. For the second 2^+ state (2_{II}^+), the significant $E2$ transition to the ground state and the strong transition to the (0_{III}^+) are

TABLE II. $E2$ transition strength in ^{16}O. $B(E2)$ values calculated with the present ^{12}C(AMD)+αGCM and those with the ^{12}C+α-OCM [19]. Experimental data are taken from Ref. [35].

		$B(E2)$ (e^2 fm^4)	
Initial	Final	Exp.	Ref. [19]
$2^+(6.92)$	$0^+(0)$	7.4±0.2	2.48
$2^+(6.92)$	$0^+(6.05)$	65±7	60.1
$2^+(9.84)$	$0^+(0)$	0.07±0.007	0.489
$2^+(9.84)$	$0^+(6.05)$	2.9±0.7	4.64
$2^+(11.5)$	$0^+(0)$	3.6±1.2	1.43
$2^+(11.5)$	$0^+(6.05)$	7.4±1.2	1.38
$4^+(10.4)$	$2^+(6.92)$	156±14	96.2
		Present	
2_I^+	0_I^+	3.2	
2_I^+	0_{II}^+	177	
2_{II}^+	0_I^+	45	
2_{II}^+	0_{II}^+	2.3	
2_{III}^+	0_I^+	0.08	
2_{III}^+	0_{II}^+	1.4	
2_{IV}^+	0_I^+	3.1	
2_{IV}^+	0_{II}^+	0.1	
4_I^+	2_I^+	290	

because it has the higher nodal ^{12}C(0_1^+)+α component and is regarded as the rotational member of the 0_{III}^+ as seen in the overlap amplitude in Fig. 6. Considering that the 0_{III}^+ state may correspond to the 0_4^+ state, the energy position of this band might be underestimated relatively to other excited states in the present calculation. If I adjust the 0_{III}^+ state to the 0_4^+ energy, 13.6 MeV, the band member 2_{II}^+ state is expected to appear around $E_x = 15$ MeV, but there is no corresponding 2^+ state with strong $E2$ transition to the ground state in the experimental data. The stability of the members of the higher nodal ^{12}C(0_1^+)+α state should be carefully checked by taking into account the coupling with continuum states. If I exclude the 2_{II}^+ from the low-energy spectra and assign the third and the fourth 2^+ states (2_{III}^+ and 2_{IV}^+) obtained in the present calculation to the 2_2^+ and 2_3^+ states, the calculated $B(E2)$ values are in reasonable agreement with the experimental ones.

In the energy region around $E_x \sim 20$ MeV, I find 2^+ states and 4^+ states having rather strong (sequential) $E2$ transition strength toward the 0_V state. In this energy region, there are several 2^+ and 4^+ states having non-negligible component of the ^{12}C(0_2^+)+α structure. I also obtain another 0^+ state with some ^{12}C(0_2^+)+α component at 20.3 MeV, a few MeV above the 0_V state. In Fig. 4, the energy levels of these states are shown by solid lines. $E2$ transition strength is fragmented among them as shown in the figure.

Figure 5 shows the overlap of those states with the ^{12}C(0_2^+)+α wave function as function of the intercluster distance d. The 0_V^+ state has more than 60%^{12}C(0_2^+)+α component at $d_\alpha = 4$–5 fm. As the spin increases, the ^{12}C(0_2^+)+α component decreases and seems scattered into several 2^+ and 4^+ states. It may imply that the structure changes; in other words, the state mixing occurs in the rotation of the ^{12}C(0_2^+)+α structure.

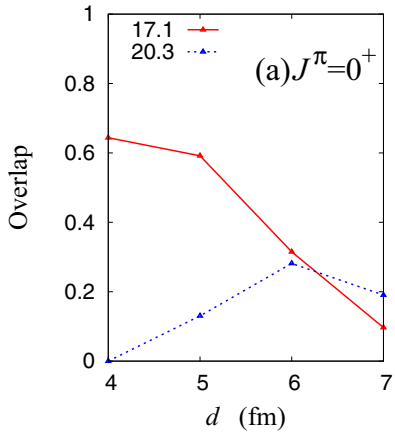

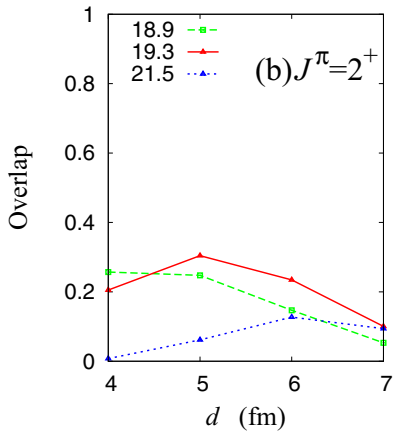

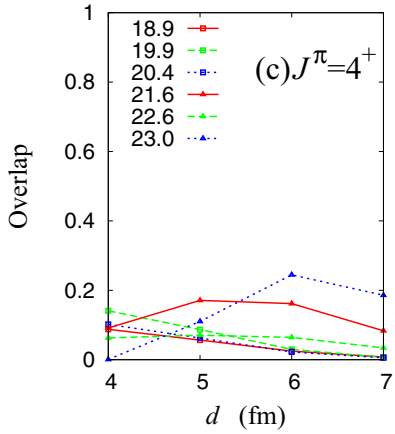

FIG. 5. (Color online) The overlap of the excited ^{16}O states with the ^{12}C(0_2^+)+α wave function as a function of the intercluster distance d defined in Eq. (9). The calculated overlap for the 0^+ states at 17.1 and 20.3 MeV, 2^+ states at 18.9, 19.3, and 21.5 MeV, and 4^+ states at 18.9, 19.9, 20.4, 21.6, 22.6, and 23.0 MeV, which have significant ^{12}C(0_2^+)+α component, is shown.

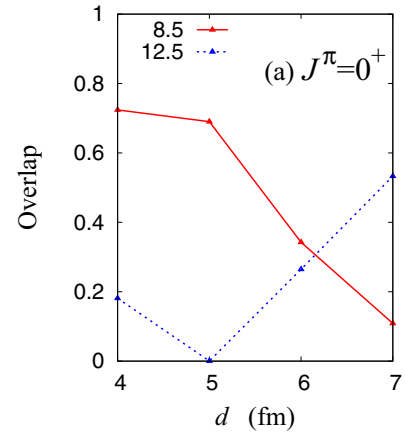

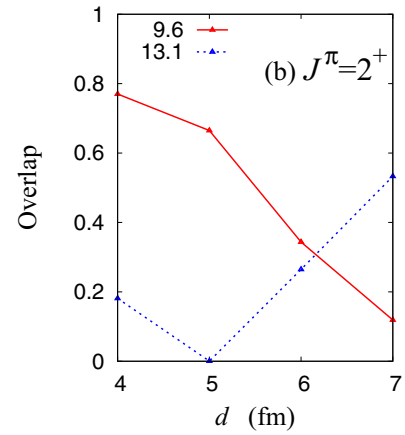

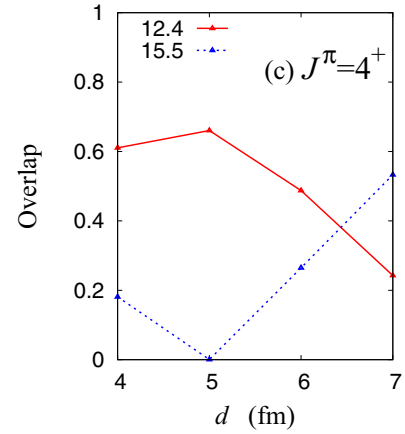

FIG. 6. (Color online) The overlap of the ^{16}O states with the ^{12}C(0_1^+)+α wave function as a function the intercluster distance d defined in Eq. (9). The overlap for the 0_{II}^+ at 8.5 MeV, 2^+ at 9.6 MeV, and 4^+ at 12.4 MeV in the ^{12}C(0_1^+)+α band, and the 0_{III}^+ at 12.5 MeV, 2^+ at 13.1 MeV, and 4^+ at 15.5 MeV in the higher nodal ^{12}C(0_1^+)+α band is shown.

I also show in Fig. 6 the overlap with the ^{12}C(0_1^+)+α wave function in the member states of the rotational bands starting from the 0_{II}^+ and 0_{III}^+ states. As seen in the figure, the lower band build on the 0_{II}^+ has the ^{12}C(0_1^+)+α structure and the higher band from the 0_{III}^+ shows the higher nodal feature of the ^{12}C(0_1^+)+α structure. The overlap with the ^{12}C(0_1^+)+α wave function in these states does not depend so much on the spin and it is still significant even in the 4^+ states.

Thus, the situation is quite different between the ^{12}C(0_1^+)+α cluster bands and the ^{12}C(0_2^+)+α bands. The instability of the ^{12}C(0_2^+)+α states in the rotation is not surprising because the ^{12}C(0_2^+) cluster is considered to be the 3α cluster gas and such a gas state should not be a rigid but fragile one differently from the ^{12}C(0_1^+) cluster.

Consequently, it is difficult to clearly identify the band members of the ^{12}C(0_2^+)+α cluster state; however, considering

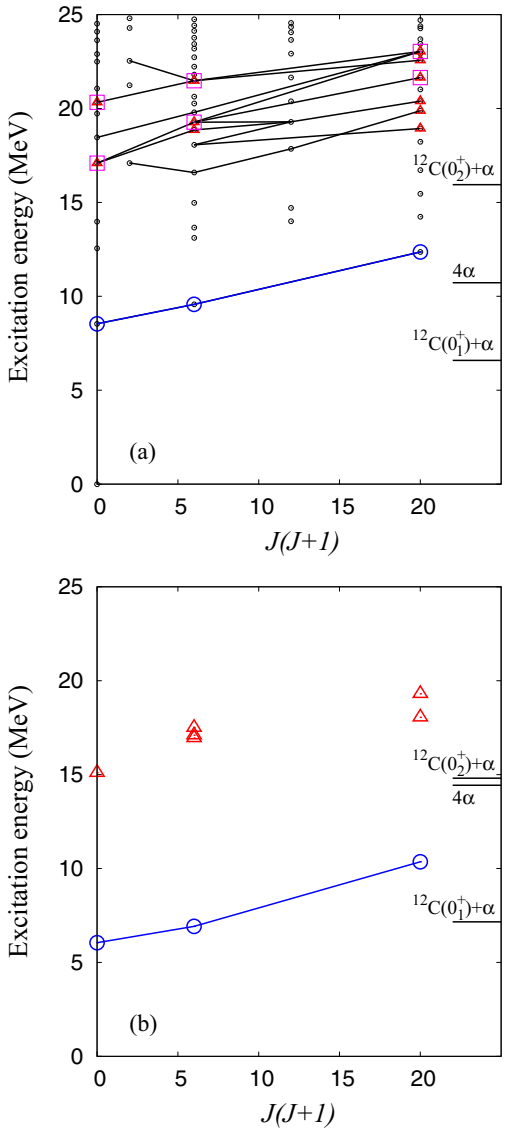

FIG. 7. (Color online) (a) Theoretical excitation levels of ^{16}O calculated with the ^{12}C(AMD)+αGCM (circles). Excited states with significant ^{12}C(0_2^+)+α component are shown by red triangles and squares. States connected by the lines are those which can be connected to the 4^+ states with the ^{12}C(0_2^+)+α component by the strong (sequential) transitions. Squares indicate possible band assignment for the ^{12}C(0_2^+)+α cluster states. Circles show the band members of the ^{12}C(0_1^+)+α cluster structure starting from the 0_{II}^+ state. (b) Experimental excitation energies of the candidate states for the ^{12}C(0_2^+)+α cluster states observed by the ^{12}C(^{12}C,^{8}Be+^{8}Be) and the ^{12}C(^{16}O, 4α) reactions [39,40], and those of the band members of the ^{12}C(0_1^+)+α structure [35].

the relatively strong $E2$ transition strength and similarity of the d dependence of the ^{12}C(0_2^+)+α overlap, I propose a possible assignment that the 2^+ state at 19.3 MeV and 4^+ at 21.6 MeV can be regarded as the band members from the 0_V^+ state, and the 2^+ state at 21.5 MeV and 4^+ at 23.0 MeV are interpreted as members of the band staring from the 0^+ state at 21.3 MeV. The excitation energies are plotted as a function of the spin $J(J+1)$ in Fig. 7. Square points indicate the assigned states, triangles show the states with significant ^{12}C(0_2^+)+α component, and circles show the rotational members of the ^{12}C(0_1^+)+α band starting from the 0_{II}^+ state. Reflecting the structure change, the slope of the energy for $J(J+1)$ does not show the linear dependence but it becomes gentle with the increase of spin. I also show in Fig. 7 the experimental energy levels of the excited states observed in the ^{12}C(^{12}C,^{8}Be+^{8}Be) and the ^{12}C(^{16}O, 4α) reactions [39,40], which are considered to be candidates for the ^{12}C(0_2^+)+α cluster states [17]. The calculated energies of the ^{12}C(0_2^+)+α states measured from the ^{12}C(0_2^+)+α threshold in the present result qualitatively agree with those of the experimental data.

IV. ISOSCALAR MONOPOLE EXCITATION

As discussed recently, isoscalar monopole (ISM) excitation in the low-energy part gives important information on cluster structures of excited states in light nuclei [24,41]. As is well known, the isoscalar giant monopole resonances (ISGMRs) in heavy nuclei have been observed as a single peak and described by the collective breathing mode. The systematics of the peak position has been discussed in association with the nuclear compressibility. In light nuclei such as ^{12}C and ^{16}O, however, it has been revealed by the (e,e') and (α,α') scattering experiments [42,43] that the ISM strength is strongly fragmented and significant fraction of the energy-weighted sum rule concentrates on a few states in a low-energy region. Recently, Yamada *et al.* discussed the ISM excitation in ^{16}O and showed that the significant ISM strength at the low-energy part up to $E_x \sim 16$ MeV can be described well by the monopole excitation to the cluster states [24]. It was argued that two different types of monopole excitation exist in ^{16}O, that is, the monopole excitation to cluster states dominating the strength in the lower-energy part and that of the mean-field type $1p$-$1h$ excitation yielding the strength in the higher-energy part $16 \leqslant E_x \leqslant 40$ MeV.

In principle, these two modes are not decoupled from but should couple to each other because the cluster excitation partially involves the $1p$-$1h$ excitation. Indeed, the monopole strength is partially described by the breathing type radial oscillation of four α clusters as suggested by a simple calculation to study the monopole oscillation using the time-dependent AMD and fermionic molecular dynamics (FMD) models [44]. Therefore, it is expected that the low-lying cluster states feed the strength of a part of the ISGMR strength originally concentrating at the higher energy region.

Although the cluster model calculations such as the 4α-OCM are useful to describe the cluster excitation, they are not enough to describe the mean-field type $1p$-$1h$ excitation because frozen 4α clusters are assumed. Also the present calculation of the ^{12}C(AMD)+α may not be sufficient for the $1p$-$1h$ excitation because an α cluster around ^{12}C is assumed in the model though twelve nucleon dynamics is incorporated in the wave function of the ^{12}C AMD wave functions. Instead of cluster model calculations, mean-field calculations including particle-hole excitations such as the random phase approximation (RPA) have been applied to investigate ISGMR. In the RPA calculations for ^{16}O [45–48], it was found that monopole strength spreads out and has a multipeak structure

with the centroid around $E_x = 20 \sim 25$ MeV. They describe the experimental strength in the high-energy region $E_x \geqslant 16$ MeV measured by (α,α') scattering. However, the peak structure with the significant fraction of the energy-weighted sum rule (EWSR) in the low-energy part is not reproduced by the mean-field calculations.

To take into account the coexistence of cluster and mean-field features in the ISM excitation, I extend our present framework of the ^{12}C(AMD)+αGCM by incorporating the $1p$-$1h$ type excitations on the top of the approximate ground state wave function obtained by the ^{16}O(AMD+VAP) calculation. After explaining the additional basis wave functions, I discuss the monopole transition in ^{16}O.

A. AMD+VAP calculation of ^{16}O and the shifted AMD method

The present method of the ^{12}C(AMD)+αGCM is suitable mainly to describe various types of cluster excitation. To take into account the $1p$-$1h$ excitation, I perform the AMD+VAP calculation for ^{16}O and consider small variations of single-particle wave functions from the obtained ground state wave function. In a similar way to Eq. (1) for ^{12}C, an AMD wave function for ^{16}O is written by a Slater determinant of 16 single-nucleon Gaussian wave packets,

$$\Phi^{\rm AMD}_{^{16}{\rm O}}(\mathbf{Z}) = \frac{1}{\sqrt{A!}}\mathcal{A}\{\varphi_1,\varphi_2,...,\varphi_A\}. \tag{11}$$

In the AMD+VAP method, the energy variation is done with respect to the spin-parity eigen wave function $P^{J\pi}_{MK}\Phi^{\rm AMD}_{^{16}{\rm O}}(\mathbf{Z})$. After the AMD+VAP calculation for ^{16}O, I get the optimum AMD solution $\Phi^{\rm AMD}_{^{16}{\rm O}}(\mathbf{Z}_0)$ which is approximately regarded as the intrinsic wave function of the ground state. Here $\mathbf{Z}_0$ indicates the set of optimized parameters $\mathbf{Z}_0 = \{\mathbf{X}^0_1,\mathbf{X}^0_2,\ldots,\mathbf{X}^0_A,\xi_1,\ldots,\xi_A\}$.

Then, I vary the spatial part of each single-particle wave function from the AMD wave function, $\Phi^{\rm AMD}_{^{16}{\rm O}}(\mathbf{Z}_0)$, by shifting a Gaussian center of the ith single-particle wave function, $\mathbf{X}^0_i \to \mathbf{X}^0_i + \delta\mathbf{e}_\sigma$ $(\sigma = 1,2,3)$. ($\mathbf{e}_1$, $\mathbf{e}_2$ and $\mathbf{e}_3$ are the three-dimension unit vectors.) For all single-particle wave functions, I consider a small shift to three directions independently, namely, $A\times 3$ kinds of shifted wave functions $\Phi^{\rm AMD}_{^{16}{\rm O}}(\mathbf{Z}'_0(i,\sigma))$ $(i = 1,\ldots,A$ and $\sigma = 1,2,3)$ with $\mathbf{Z}'_0(i,\sigma) \equiv \{\mathbf{X}^{0'}_1,\ldots,\mathbf{X}^{0'}_i + \delta\mathbf{e}_\sigma,\ldots,\mathbf{X}^{0'}_A,\xi_1,\ldots,\xi_A\}$. Here $\mathbf{X}^{0'}_A$ is chosen to be $\mathbf{X}^{0'}_A = \mathbf{X}^0_A - \delta\mathbf{e}_\sigma/A$ to take into account the recoil effect. By using the linear combination of $1 + 16\times 3 = 49$ wave functions, the original wave function $\Phi^{\rm AMD}_{^{16}{\rm O}}(\mathbf{Z}_0)$ and the shifted ones $\Phi^{\rm AMD}_{^{16}{\rm O}}(\mathbf{Z}'_0(i,\sigma))$, $1p$-$1h$ excitations in the intrinsic frame are incorporated. I fix the spin orientations ξ_i and consider the $1p$-$1h$ excitations mainly for the spatial part. For excited 0^+ states of ^{16}O, I superpose the spin-parity eigenstates projected from those wave functions, $P^{J\pi}_{MK}\Phi^{\rm AMD}_{^{16}{\rm O}}(\mathbf{Z}_0)$ and $P^{J\pi}_{MK}\Phi^{\rm AMD}_{^{16}{\rm O}}(\mathbf{Z}'_0(i,\sigma))$. The coefficients of each basis wave functions are determined by diagonalizing the norm and Hamiltonian matrices. By adopting a small enough value for the shift parameter δ, I perform the small amplitude limit calculation with the AMD framework. In the present work, I take the parameter $\delta = 0.1$ which is small enough to get the δ-independent result after the diagonalization. I call this calculation "^{16}O(shifted AMD)". If arbitrary variation of the single-particle wave functions is taken into account, the small-amplitude calculation in the intrinsic frame contains $1p$-$1h$ excitation modes and corresponds to the RPA calculation. However, in the present calculation based on the shifted AMD, the variation of a single-particle wave function is restricted only in the shift of Gaussian wave packet and the spin variation is omitted. It means that the model space of the shifted AMD partially covers the model space of $1p$-$1h$ excitations. Owing to the spin and parity projections, higher order excitations beyond $1p$-$1h$ such as the coupling of the single-particle excitation with the rotational mode can be contained in the present framework of the shifted AMD.

In addition to the ^{16}O(shifted AMD) calculation, I also perform the hybrid calculation of ^{12}C(AMD)+αGCM and ^{16}O(shifted AMD) by superposing all basis wave functions. The coefficients are determined again by the diagonalization.

B. Monopole transitions

The strength function of the ISM excitation from the ground state of ^{16}O is

$$S(E) \equiv \delta(E - E_n)|M(IS0,0^+_1 \to 0^+_n)|^2, \tag{12}$$

$$M(IS0,0^+_1 \to 0^+_n) = \langle 0^+_n|\sum_{i=1}^{16}\mathbf{r}_i^2|0^+_1\rangle. \tag{13}$$

For the isoscalar excitation, this is 4 times as much as the isoscalar $E0$ strength function defined in Refs. [42,43]. The EWSR of the ISM transition is

$$\sum_n (E_n - E_1)|M(IS0,0^+_1 \to 0^+_n)|^2 = \frac{2\hbar^2}{m}16\langle r^2\rangle, \tag{14}$$

where $\langle r^2\rangle$ is the mean-square matter radius of the ground state,

$$\langle r^2\rangle = \frac{1}{16}\langle 0^+_1|\sum_{i=1}^{16}\mathbf{r}_i^2|0^+_1\rangle. \tag{15}$$

In the results of the ^{12}C(AMD)+αGCM, the ^{16}O(shifted AMD), and the hybrid of ^{12}C(AMD)+αGCM and ^{16}O(shifted AMD), the energy-weighted sum of the ISM strength for all excited states is 93%, 87%, and 95% of the EWSR value, respectively.

Since the present calculation is the bound state approximation where coupling with continuum states is omitted, all excited states are discrete states without escaping width. Nevertheless, the monopole strengths calculated in the bound state approximation may be helpful to discuss the gross structure of the monopole strength and also useful to analyze the contribution from each mode qualitatively, provided that such characteristic modes of monopole excitations as collective breathing modes and cluster excitation ones keep their features under the coupling with continuum states. For quantitative discussions of monopole strength function such as the energy position and width of monopole resonances in the high-energy region, one should carefully take into account the coupling with continuum states.

I calculate the ISM transition matrix element $M(IS0)$ for 0^+_n states of the ^{12}C(AMD)+αGCM, the ^{16}O(shifted AMD),

and the hybrid full calculations. The calculated ISM transition strength $[B(IS0) = |M(IS0)|^2]$ is shown in the histogram in Fig. 8, where the strength $|M(IS0)|^2$ for 0_n^+ states in each energy bin is summed up.

In the ^{12}C(AMD)+αGCM result, the significant strength exists in the low-energy part for the 0_{II}^+, 0_{III}^+, and 0_{IV}^+ states having the ^{12}C$(0_1^+,2_1^+)+\alpha$ cluster structures. They exhaust $\sim$30% of the EWSR. Such a large fraction in the low-energy part ($E_x \leqslant 16$ MeV) is comparable to the 4α-OCM calculation where $\sim$20% of the EWSR exists in the $E_x \leqslant 16$ MeV part [24].

In the result of the ^{16}O(shifted AMD) calculation, the ISM transition strength shows the two-peak structure around $E_x \sim 20$ MeV, one below and the other above $E_x = 20$ MeV. The lower and the higher peaks exhaust about 20% and 40% of the EWSR, respectively. The lower peak is understood as the motion of one α cluster against the ^{12}C core, namely, the coherent mode of four single-particle motions against the residual 12 nucleons. This mode originates in the ground state α correlation around the ^{12}C core contained in the AMD+VAP result of ^{16}O(0_1^+). The EWSR ratio for the lower peak is the same order of the EWSR ratio for the cluster states with the ^{12}C$(0_1^+,2_1^+)+\alpha$ cluster structures in $E_x \leqslant 16$ MeV calculated with the ^{12}C(AMD)+αGCM. On the other hand, the higher peak around 25 MeV corresponds to the breathing mode which can be described by the coherent isotropic single-particle motions. This peak consists of two excited states which almost degenerate within 1 MeV. Comparing with the RPA and the second RPA calculations [46,48] that show three bump structure having spreading widths, the present calculation describes only three simple states without fragmentation, maybe because of the restriction of the present model space.

The full calculation using the hybrid model space of the ^{12}C(AMD)+αGCM and the ^{16}O(shifted AMD) shows qualitatively similar features of the ^{12}C(AMD)+αGCM calculation. Namely, there exist three peaks corresponding to the cluster states in the low-energy part ($E_x \leqslant 16$ MeV) exhausting $\sim$25% of the EWSR, and the concentration of the strength around the peak-like structure slightly above 20 MeV. Quantitatively, the monopole strengths of 0^+ states in the low-energy part are somehow different between two calculations. In particular, the strengths of the third and fourth states (0_{III}^+ and 0_{IV}^+) having the higher nodal ^{12}C$(0_1^+)+\alpha$ component and the ^{12}C$(2_1^+)+\alpha$ one change because these two components mix to each other in the present calculation. Qualitatively, however, the effect of $1p$-$1h$ excitation modes to the monopole strengths for cluster states is minor. This result is consistent with the work by Suzuki and Hara with the calculation of the ^{12}C+α cluster and symplectic mixed basis [49].

Comparing the results of the ^{12}C(AMD)+αGCM, the ^{16}O(shifted AMD), and the full hybrid calculations, it is found that there is no significant difference of the EWSR ratios of the low-energy and high-energy parts among three calculations. This implies that two modes around $\sim$20 MeV obtained in the ^{16}O(shifted AMD) are involved in excited states of the ^{12}C(AMD)+αGCM. That is, the higher peak of the collective breathing mode corresponds to the peak-like structure slightly above 20 MeV in the ^{12}C(AMD)+αGCM and the full calculation, while the lower mode for the ^{12}C-α

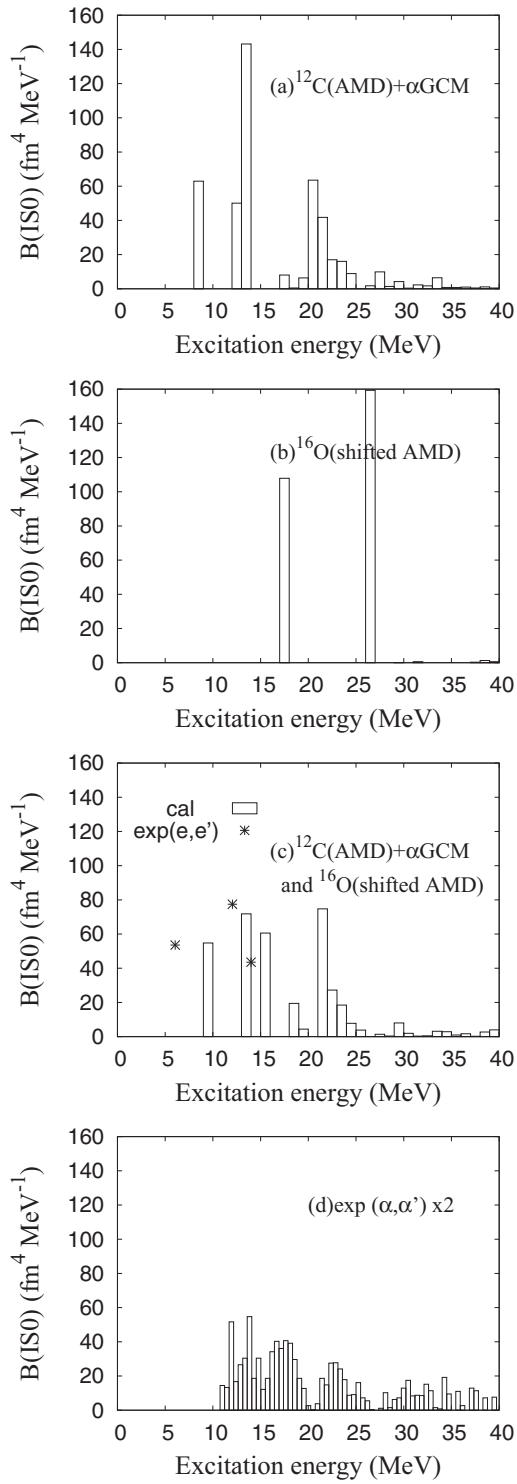

FIG. 8. Isoscalar monopole transition strength function. The theoretical $B(IS0)$ calculated with (a) the ^{12}C(AMD)+αGCM, (b) the ^{16}O(shifted AMD), and (c) the hybrid of ^{12}C(AMD)+αGCM and ^{16}O(shifted AMD). In the histogram the strength in each energy bin is summed up. The experimental $B(IS0)$ (fm^4) converted from the $B(E0)$ measured by (e,e') scattering for the 0^+ states at 6.05 MeV, 12.05 MeV, and 14.01 MeV are also shown by stars in the third panel (c). (d) The experimental data measured by (α,α') scattering. I multiply the data from Ref. [43] by a factor 2 in panel (d).

motion is fragmented in the lowest three excited 0^+ states with the ^{12}C(0^+_1,2^+_1)+α cluster structures. Namely, I can make the following conclusions regarding the origins of isoscalar monopole excitations: In the mean-field type $1p$-$1h$ excitation described by the shifted AMD, there exist two modes around $E_x \sim 20$ MeV. The lower mode corresponds to the ^{12}C-α relative motion and the higher one is the collective breathing mode. The former is described by the coherent mode of four single-particle motions against residual 12 nucleons and the latter is the coherent isotropic mode of all single-particle motions in the shifted AMD calculation. Because of the coupling with the cluster excitation, the lower mode is fragmented into several cluster states in $E_x \leqslant 16$ MeV while lowering the energy centroid. The strength of the higher breathing mode is somehow spread and also its energy centroid is lowered to contribute to the strength around $E_x \sim 20$ MeV. The present result is consistent with the suggestion of two different-type excitation modes in the isoscalar monopole transitions in ^{16}O by Yamada *et al*. in Ref. [24].

The ISM transition strength has been observed by (α,α') scattering [43]. The measured strength for the 0^+ states at 12 and 14 MeV is smaller than the that observed by (e,e') scattering by a factor 2–4. Moreover, their measurement in the energy region $11 < E_x < 40$ MeV yields only ∼50% of the $E0$ EWSR. These facts may suggest possible ambiguity of the normalization in the ISM strength measured by (α,α') scattering. I multiply the experimental data by a factor 2 and show the values in Fig. 8(d) to compare the shape of the strength function with our result. Comparing the result of the full calculation with the experimental data, it is shown that the strength for the 0^+_{III} and 0^+_{IV} states at 13 and 15 MeV may describe the peaks in the $11 < E_x < 16$ MeV of the experimental data. The significant strength in the higher region around 20 MeV is considered to correspond to the bump structures in the regions $16 < E_x < 20$ MeV and/or $20 < E_x < 25$ MeV. The calculated strengths are not fragmented as much as the experimental ones, maybe because of the limitation of the present model space.

V. SUMMARY AND OUTLOOK

Cluster structures and monopole transitions in positive parity states of ^{16}O were investigated based on the ^{12}C(AMD)+αGCM calculation. The lowest three excited 0^+ states (0^+_{II}, 0^+_{III}, and 0^+_{IV}) have the ^{12}C(0^+_1,2^+_1)+α cluster structures. The 0^+_{II} with the ^{12}C(0^+_1)+α structure and its rotational band members qualitatively reproduce the properties such as energy levels and $E2$ and monopole transition strengths for the experimental 0^+_2, 2^+_1, and 4^+_1 states, which have been considered to be the ^{12}C(0^+_1)+α cluster band. As far as I know, the present calculation is the first microscopic calculation that can describe reasonably the excitation energies of these excited states.

In the present calculation, I obtained the fifth 0^+ state (0^+_V) having the developed ^{12}C(0^+_2)+α structure. Because of the feature that an α cluster is moving in the $L = 0$ wave around the ^{12}C(0^+_2), it is regarded as the 4α cluster gas state similar to the 3α cluster gas in the ^{12}C(0^+_2). This state may correspond to the 0^+_6 state of the 4α cluster gas state suggested in the 4α-OCM by Funaki *et al*. [5,6].

With the analyses of the $E2$ transition strength and the ^{12}C(0^+_2)+α component, I considered band members of the ^{12}C(0^+_2)+α cluster state. Around $E_x \sim 20$ MeV, there are several 2^+ and 4^+ states having some component of ^{12}C(0^+_2)+α. The $E2$ transition strength is fragmented among them. The present result suggests that the structure changes; in other words, the state mixing occurs in the rotation of the ^{12}C(0^+_2)+α cluster structure. This makes it difficult to assign clearly the ^{12}C(0^+_2)+α band members in high spin states. This feature is different from that of the ^{12}C(0^+_1)+α cluster band and may originate in the 3α cluster gas feature of the ^{12}C(0^+_2) that might be fragile in the rotation.

The isoscalar monopole excitation was discussed with the ^{12}C(AMD)+αGCM and also with the hybrid calculation of the ^{12}C(AMD)+αGCM and ^{16}O(shifted AMD). In the strength of both calculations, there exist three peaks for the cluster states in the low-energy part ($E_x < 16$ MeV). This is consistent with the preceding work with the 4α-OCM calculation [24]. I also found the concentration of the strength around the peak-like structure slightly above $E_x \sim 20$ MeV, which originates in the collective breathing mode. Comparing the hybrid calculation with the ^{16}O(shifted AMD) calculation, I make the following conclusions regarding the origins of isoscalar monopole excitations: In the mean-field type $1p$-$1h$ excitation described by the shifted AMD, there exist two modes around $E_x = 20$ MeV. The lower mode corresponds to the ^{12}C-α relative motion and the higher one is the collective breathing mode. The former is described by the coherent mode of four single-particle motions against the residual 12 nucleons and the latter is the coherent isotropic mode of all single-particle motions in the shifted AMD calculation. In the hybrid calculation, because of the coupling with the cluster excitation, the lower mode is fragmented into several cluster states in $E_x < 16$ MeV while lowering the energy centroid. The higher-energy breathing mode is somehow spread and its energy centroid is lowered to contribute to the strength around $E_x \sim 20$ MeV. The present result is consistent with the suggestion of two different-type excitation modes in the isoscalar monopole transitions in Ref. [24].

The present calculation is a bound state approximation. The stability of the excited states should be studied in more detail by taking into account coupling with continuum states. Also for the quantitative discussion of monopole strength function, it is important to consider the coupling with continuum states. I also should reexamine the choice of the effective interaction and the interaction parameters for quantitative reproduction of energy levels. In the present work, I used the same phenomenological effective nuclear forces as those used in the previous work on ^{12}C. The energy spectra of ^{16}O may be improved by fine tuning of the interaction parameters. However, I have some difficulty in completely reproducing the binding energies of α, ^{12}C, and ^{16}O as well as the energy spectra of the subsystem ^{12}C simultaneously with such phenomenological effective nuclear interaction. *Ab initio* calculation based on realistic nuclear force is one of the promising tools for quantitative prediction of energy spectra of ^{16}O, though applications of *ab initio* calculations to cluster states are still limited.

ACKNOWLEDGMENTS

The author would like to thank Dr. Funaki and Dr. Yamada for fruitful discussions. The computational calculations of this work were performed by using the supercomputers at YITP. This work was supported by a Grant-in-Aid for Scientific Research from the Japan Society for the Promotion of Science (JSPS). It was also supported by a Grant-in-Aid for the Global COE Program "The Next Generation of Physics, Spun from Universality and Emergence" from the Ministry of Education, Culture, Sports, Science, and Technology (MEXT) of Japan.

[1] A. Tohsaki, H. Horiuchi, P. Schuck, and G. Ropke, Phys. Rev. Lett. **87**, 192501 (2001).
[2] Y. Funaki, H. Horiuchi, A. Tohsaki, P. Schuck, and G. Ropke, Prog. Theor. Phys. **108**, 297 (2002).
[3] T. Yamada and P. Schuck, Phys. Rev. C **69**, 024309 (2004).
[4] Y. Funaki, A. Tohsaki, H. Horiuchi, P. Schuck, and G. Ropke, Phys. Rev. C **67**, 051306 (2003).
[5] Y. Funaki, T. Yamada, H. Horiuchi, G. Ropke, P. Schuck, and A. Tohsaki, Phys. Rev. Lett. **101**, 082502 (2008).
[6] Y. Funaki, T. Yamada, A. Tohsaki, H. Horiuchi, G. Ropke, and P. Schuck, Phys. Rev. C **82**, 024312 (2010).
[7] T. Yamada, Y. Funaki, H. Horiuchi, G. Roepke, P. Schuck, and A. Tohsaki, in *Clusters in Nuclei, Vol. 2*, Lecture Notes in Physics, Vol. 848, edited by C. Beck (Springer, Berlin, 2012), p. 229.
[8] Y. Kanada-En'yo, Phys. Rev. C **75**, 024302 (2007).
[9] Y. Kanada-En'yo, Phys. Rev. C **76**, 044323 (2007).
[10] N. Itagaki, M. Kimura, C. Kurokawa, M. Ito, and W. von Oertzen, Phys. Rev. C **75**, 037303 (2007).
[11] T. Yamada and Y. Funaki, Phys. Rev. C **82**, 064315 (2010).
[12] T. Suhara and Y. Kanada-En'yo, Phys. Rev. C **85**, 054320 (2012).
[13] T. Ichikawa, N. Itagaki, Y. Kanada-En'yo, T. Kokalova, and W. von Oertzen, Phys. Rev. C **86**, 031303 (2012).
[14] F. Kobayashi and Y. Kanada-En'yo, Phys. Rev. C **86**, 064303 (2012).
[15] F. Kobayashi and Y. Kanada-En'yo, arXiv:1305.4323.
[16] T. Wakasa, E. Ihara, K. Fujita, Y. Funaki, K. Hatanaka, H. Horiuchi, M. Itoh, J. Kamiya *et al.*, Phys. Lett. B **653**, 173 (2007).
[17] S. Ohkubo and Y. Hirabayashi, Phys. Lett. B **684**, 127 (2010).
[18] Y. Funaki, T. Yamada, H. Horiuchi, G. Roepke, P. Schuck, and A. Tohsaki, Prog. Theor. Phys. Suppl. **196**, 439 (2012).
[19] Y. Suzuki, Prog. Theor. Phys. **55**, 1751 (1976); **56**, 111 (1976).
[20] M. Libert-Heinemann, D. Baye, and P.-H. Heenen, Nucl. Phys. A **339**, 429 (1980).
[21] K. Ikeda, H. Horiuchi, and S. Saito, Prog. Theor. Phys. Suppl. **68**, 1 (1980).
[22] S. Saito, Prog. Theor. Phys. **40**, 893 (1968); **41**, 705 (1969); Prog. Theor. Phys. Suppl. **62**, 11 (1977).
[23] K. Fukatsu and K. Katō, Prog. Theor. Phys. **87**, 151 (1992).
[24] T. Yamada, Y. Funaki, T. Myo, H. Horiuchi, K. Ikeda, G. Ropke, P. Schuck, and A. Tohsaki, Phys. Rev. C **85**, 034315 (2012).
[25] J. A. Wheeler, Phys. Rev. **52**, 1083 (1937).
[26] D. L. Hill and J. A. Wheeler, Phys. Rev. **89**, 1102 (1953); J. J. Griffin and J. A. Wheeler, *ibid.* **108**, 311 (1957).
[27] Y. Kanada-En'yo, H. Horiuchi, and A. Ono, Phys. Rev. C **52**, 628 (1995); Y. Kanada-En'yo and H. Horiuchi, *ibid.* **52**, 647 (1995).
[28] Y. Kanada-En'yo and H. Horiuchi, Prog. Theor. Phys. Suppl. **142**, 205 (2001); Y. Kanada-En'yo, M. Kimura, and H. Horiuchi, C. R. Phys. **4**, 497 (2003); Y. Kanada-En'yo, M. Kimura, and A. Ono, Prog. Theor. Exp. Phys. **2012**, 01A202 (2012).
[29] Y. Kanada-En'yo, Phys. Rev. Lett. **81**, 5291 (1998).
[30] Y. Kanada-En'yo, Prog. Theor. Phys. **117**, 655 (2007); **121**, 895 (2009).
[31] T. Ando, K. Ikeda, and A. Tohsaki, Prog. Theory. Phys. **64**, 1608 (1980).
[32] K. Minomo, T. Sumi, M. Kimura, K. Ogata, Y. R. Shimizu, and M. Yahiro, Phys. Rev. Lett. **108**, 052503 (2012).
[33] Y. Kanada-En'yo, Phys. Rev. C **85**, 044320 (2012).
[34] N. Yamaguchi, T. Kasahara, S. Nagata, and Y. Akaishi, Prog. Theor. Phys. **62**, 1018 (1979); R. Tamagaki, *ibid.* **39**, 91 (1968).
[35] D. R. Tilley, H. R. Weller, and C. M. Cheves, Nucl. Phys. A **564**, 1 (1993).
[36] I. Angeli, At. Data Nucl. Data Tables **87**, 185 (2004).
[37] F. Ajzenberg-Selove, Nucl. Phys. A **460**, 1 (1986).
[38] T. Yamada and P. Schuck, Eur. Phys. J. A **26**, 185 (2005).
[39] P. Chevallier, F. Scheibling, G. Goldring, I. Plesser, and M. W. Sachs, Phys. Rev. **160**, 827 (1967).
[40] M. Freer, N. M. Clarke, N. Curtis, B. R. Fulton, S. J. Hall, M. J. Leddy, J. S. Pople, G. Tungate *et al.*, Phys. Rev. C **51**, 1682 (1995).
[41] T. Yamada, Y. Funaki, H. Horiuchi, K. Ikeda, and A. Tohsaki, Prog. Theor. Phys. **120**, 1139 (2008).
[42] M. W. Krison, Nucl. Phys. A **257**, 58 (1976).
[43] Y.-W. Lui, H. L. Clark, and D. H. Youngblood, Phys. Rev. C **64**, 064308 (2001).
[44] T. Furuta, K. H. O. Hasnaoui, F. Gulminelli, C. Leclercq, and A. Ono, Phys. Rev. C **82**, 034307 (2010).
[45] J. P. Blaizot, D. Gogny, and B. Grammaticos, Nucl. Phys. A **265**, 315 (1976).
[46] Z. Ma, N. Van Giai, H. Toki, and M. L'Huillier, Phys. Rev. C **55**, 2385 (1997).
[47] P. Papakonstantinou and R. Roth, Phys. Lett. B **671**, 356 (2009).
[48] D. Gambacurta, M. Grasso, and F. Catara, Phys. Rev. C **81**, 054312 (2010).
[49] Y. Suzuki and S. Hara, Phys. Rev. C **39**, 658 (1989).